S^3 - SENTINEL SYNERGY STUDY

Prototype retrieval algorithms based on synergistic use of Microwave and Optical imagers for land

Deliverable D9
Executive Summary

prepared by

in co-operation with

Contract:	4000119682
Title:	Executive Summary
Version	1.0 Initial Version

Change-Log

Version	Date	Change
1.0	27.03.2019	Initial submission

Summary

This document is the Executive Summary of the Sentinel-Synergy-Study funded by ESA under contract 4000119682. It is an unformatted version of paper which will be submitted to the Journal "Remote Sensing of Environment"

1 Introduction

With the launch of the first Sentinel satellites, a new era in Earth Observation has started that allows for the development of new approaches that use these novel observations at high temporal frequencies and fine spatial resolution with complementary information from the optical and microwave spectral domains. One very important application for is the monitoring of crops.

Optical remote sensing of crops and crop yields has a long history, stretching back as nearly far as the advent of satellite remote sensing itself (e.g. Idso et al. 1977, Tucker 1980). Most early examples use vegetation indices (primarily NDVI — the Normalised Difference Reflectance Index) from AVHRR or Landsat data and calibrate empirical relationships with variables such as yield or leaf area. Indeed, even today the majority of studies using optical remote sensing data to monitor crops continue to focus on the use of vegetation indices. For example, NDVI for yield determination in soybean (Liu and Kogan, 2002), PVI for determining faPAR in corn (Weigand et al. 1986), LAI from RVI in maize (Gardber and Blad, 1986) and TSAVI for determining green crop area in wheat (Broge and Mortensen, 2002). Vina et al. (2011) compared a large number of vegetation indices to estimate the leaf area index of maize and soybean and found that those designed to be sensitive to chlorophyll concentration (e.g. the MERIS Terrestrial Chlorophyll Index, MTCI) gave the best predictions. The advantage of these and similar techniques is that they are relatively straight forward to apply and computationally cheap to implement. In principle they give reasonable results for the areas and cover types over which they were calibrated. However, their major shortcoming is that with little or no underlying physics they are not generalizable beyond the areas which they were calibrated and applications on an appreciable scale are unlikely to yield accurate results. In particular such techniques are not amenable to combining data from different sensors and different domains of the electromagnetic spectrum. If we want to combine data from optical sensors such as Sentinel-2 with SAR sensors such as Sentinel-1 some form of physically based model will be required.

Examples of crop remote sensing using physical models of radiative transfer in the optical domain are far less numerous than those using empirical techniques. One approach that has been used by a number of authors is to use a vegetation canopy radiative transfer (RT) model to calibrate the vegetation indices. Féret et al. (2011) used the PROSPECT-5 model to develop relationships between spectral indices and leaf pigment concentrations using partial least squares at the leaf level. The study included maize and soybean crops as well as a number of tree species. They showed that it is possible

to construct simple polynomial relationships that describe a large amount of variability in the data – however it is likely to be more complex when moving to a full canopy due to the influence of soil optical properties and the physical structure of the canopy.

The retrieval of biogeophysical parameters over agricultural landscapes also has a long tradition in microwave remote sensing. The general challenge is the separation of the different contributions of surface properties to the Synthetic Aperture Radar (SAR) signal. These typically comprise components such as soil moisture, surface roughness, vegetation water content and vegetation structural effects and need to be disentangled during a retrieval process.

Unlike in the optical domain there has been a greater focus on physical modelling for SAR applications. Attempts to describe the backscattering from vegetation covered areas have been made since the late 1970s. They have evolved from the simple "cloud" model of *Attema and Ulaby* (1978) to multilayered, multi-constituent models like the MIchigan MIcrowave Canopy Scattering Model (MIMICS) proposed by *Ulaby and Elachi* (1990) or the radiative transfer model of *Karam et al.* (1992). More complex radiative transfer (RT) models have been developed to take into account the 3-dimensional canopy structure (e.g. Floury, 1999; *Martinez et al.* (2000); *Disney and Lewis* (2003); *Lewis et al.* (2003); *Bracaglia* (1995)). Some examples of empirical indices from SAR data also exist. *Kim and van Zyl* (2001) proposed the Radar Vegetation Index (RVI), which is sensitive to the fresh biomass and vegetation water content (*Kim and Won*, 2003).

Usually vegetation biomass and LAI over agricultural fields is estimated from SAR data at high frequencies. However, from the SIR-X/C as well as multi-frequency airborne campaigns knowledge exist that L-band backscattering exhibited a high sensitivity to vegetation biomass of crops characterized by large leaves (e.g. corn and sunflowers); whereas higher frequencies (C and X bands) showed good agreement with the development of plants with narrow leaves (e.g. wheat) (*Ferrazzoli and Guerriero*, 1996; *Mattia et al.*, 2003). *Mattia et al.* (2003) used ENVISAT ASAR data for the retrieval of fresh biomass and LAI values over wheat fields by means of the HH/VV ratio and *Satalino et al.* (2006) used the same approach for the retrieval of LAI and compared results with LAI derived from in-situ data. They concluded that LAI can be retrieved with the same accuracy as with optical (MERIS) data. *McNairn et al.* (2012) used Radarsat2 data for the retrieval of LAI data and concluded that, similar to *Mattia et al.* (2003), the co–pol ratio as well as the HV/VV ratio and HV backscatter is a good estimator of LAI. However, with the availability of fully polarimetric data, they suggest the usage of H from the H, A, alpha decomposition as well as the volume component from the Freeman-Durden decomposition for the retrieval of LAI. Paloscia et al. (2012) used dual frequency X- and L-Band data for the retrieval of plant moisture content. Using an empirical model combining L-Band HH- pol and X-Band VV-pol backscatter values in dependency of the growth structure of the plants, they inverted plant moisture content within a for the season expected range and accuracy.

The advent of Sentinel–1 and Sentinel–2 in orbit at the same time provides an exciting opportunity to develop new retrieval technique to exploit the synergy's between the microwave (specifically SAR) and optical domains. Because of a historical lack of contemporaneous observations in these domains the combination of SAR and optical

instruments for crop monitoring is less common than the use of either one on its own but the potential of this combination to provide information to crop models is significant as the two types of observations contain very different and complementary information. *Prévot et al.* (2003) present one of the few examples; they used PROSAIL and the zero order SAR model of *Attema and Ulaby* (1978) to assimilate both optical and SAR data into the STICS crop model. A small number of parameters were retrieved: the sowing date, duration of maximum LAI, the field capacity of the first soil layer and parameters that control stem density and evaporation. Interestingly the authors note that whilst the optical data improved the model outputs the SAR data did not improve the model performance. They suggest that the main reason for this is that the relatively low volumes of SAR data available made it difficult to characterise the soil moisture correctly. There is clearly the potential to improve on this situation: with the advent of Sentinel-1 the amount of SAR data available will be much greater and newer data assimilation techniques are capable of dealing with a larger number of parameters.

This paper examines synergistic retrievals from Sentinel–1 and Sentinel–2 data by inverting coupled optical and microwave radiative transfer models. The retrieval of the actual state of the land surface is typically an undetermined problem. The number of observables is typically much smaller than the number of unknown parameters in both, the optical and SAR domain. However, the SAR and optical data contain complementary information that can be exploited by advanced retrieval algorithms.

2 Data and methods

2.1 Satellite Data

Sentinel–1 and Sentinel–2 data were downloaded from the Sentinel data hub API for the sites described in Section 2.2. For Sentinel–2, level 2a surface reflectance data were acquired, resampled to a common spatial resolution and co–registered with the Sentinel–1 data using the ESA SNAP toolbox. Cloudy pixels were eliminated based on the level 2a internal cloud mask. No further pre–processing was carried out on the Sentinel–2 data.

Additional pre–processing steps for Sentinel–1 data, all using the SNAP toolbox, included thermal noise removal, radiometric correction, backscatter normalisation to account for changes in incidence angles across the swath and speckle filtering using a multi–temporal Lee filter.

2.2 Field Data

Field data were acquired as part of the Munich North Isar (MNI) campaign which takes place in farmland to the north of the city of Munich (Germany). The MNI fields used in this study are labelled 508, which is growing wheat, 515 which is goring maize and 542 which its growing triticale which is a hybrid of wheat and rye. For each field three points were sampled and are labelled in this manuscript as “low”, ”mid’ and ”high”

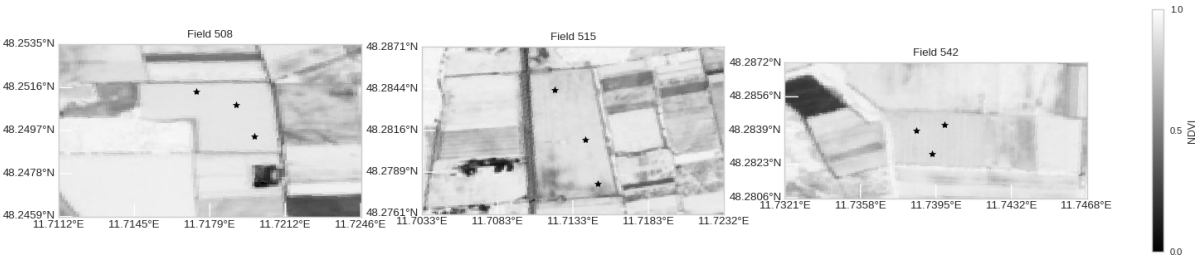

Figure 1: Sentinel–2 NDVI images of the three fields used in this study. From left to right they are growing wheat, maize and triticale. The images were acquired on the 26th of June 2017.

representing their position from South to North, The campaign started end of March 2017 and continued until harvesting of the corresponding crops. Measurements of leaf area index (LAI) and soil moisture were been carried out at the sampling locations indicated in Figure 1. LAI was measured using a Li–Corr LAI2000 instrument. Each sampling locations is equipped with a data logger (Decagon EM50) and probes (Decagon 5TM) that measure the soil moisture dynamics in 5cm, 10cm and 30cm depths with two repetitions each.

2.3 Radiative Transfer models

2.3.1 Optical Radiative Transfer

The Semi Discrete model of *N. et al.* (1997) represents canopy reflectance via the addition of three terms:

$$\rho_{canopy} = \rho^1(z_0, \Omega, \Omega_0) + \rho^0(z_0, \Omega, \Omega_0) + \rho^M(z_0, \mu, \mu_0) \tag{1}$$

where ρ_{canopy} is the canopy reflectance, ρ^1 is the reflectance from photons that have had a single interaction with the canopy ρ^0 is the reflectance due to photons that have only interacted with the soil and ρ^M is the reflectance due to photons that have had multiple interactions within the canopy, possibly including the soil. The BRDF is controlled by the first two terms and the third is assumed to be isotropic. A hotspot term is added into ρ^1 and ρ^0 to account for the enhanced probability of a photon exiting the canopy if it leaves along the same or similar path via which it entered. Leaf optical properties are prescribed using the PROSPECT model (*Jacquemoud and Baret*, 1990) and soil optical properties via the model of *Price* (1990). PROSPECT parameters were held constant at typical values for healthy cereal crops. In addition a very simple model of the impact of soil moisture on the first component of the Price reflectance spectra was included such that

$$\rho^*_{s1} = \rho_{s1}(1 - 0.5\theta_m), \tag{2}$$

where ρ_{s1} is the first orthogonal component reflectance spectra from the Price model, θ_m is the soil moisture and ρ^*_{s1} is the modified reflectance spectra. The effect of this

modification is a first order approximation to make the soil darker when it is wetter.

To convert from the top–of–canopy reflectance spectra computed by the Semi–discrete model to the wave bands of Sentinel–2 the model outputs were convolved with the spectral response functions of the instrument.

2.3.2 Microwave Radiative Transfer

For the microwave domain, the semi-empirical single scattering radiative transfer model developed by *De Roo et al.* (2001) is used to model the backscatter values of Sentinel–1. The total single-scattering pq-polarized backscattering coefficient is expressed by the following equation:

$$\sigma^0_{pq}[m^2/m^2] = \sigma^0_{g_{pq}} + \sigma^0_{c_{pq}} + \sigma^0_{gcg_{pq}} + \sigma^0_{cg_{pq}} \tag{3}$$

where each component represents a different scattering mechanism. For a particular -polarization configuration, these components are: $\sigma^0_{g_{pq}}$, the direct backscatter contribution of the underlying soil surface (including two-way attenuation by the canopy); $\sigma^0_{c_{pq}}$, direct backscatter contribution from the canopy; $\sigma^0_{gcg_{pq}}$, ground–canopy–ground scattering contribution and; $\sigma^0_{cg_{pq}}$, the combined ground–canopy and canopy–ground scattering contribution. For the soil backscattering term, $\sigma^0_{g_{pq}}$, the model of *Oh et al.* (1992) is used. The other components are modelled as a uniform water cloud following *Attema and Ulaby* (1978).

2.4 Retrieval Algorithm

To link a satellite observation to the state of the land surface, s_i, at acquisition time t_i we need a forward model or observation operator *Kaminski et al.* (2017), that simulates the satellite observations given s_i. In our case, the observation operators for S1 and S2 are provided by the models described in sections 2.3.2 and 2.3.1 respectively. We denote these observation operators by $H_b(s_i, x_b, g_b)$ and $H_o(s_i, x_o, g_o)$, using the index b for backscatter and o for optical. The vectors x_b and x_o denote uncertain parameters in the formulation of the respective observation operators while $g_{b,t}$ and $g_{o,t}$ are known variables, for example sun–sensor geometry. We formulate the retrieval by concatenating the unknown sequence of states s_i at all times t_i into one long vector s, the state trajectory. We also introduce a dynamic model that we will use to help constrain the solution. If the model was perfect, M would fulfill the equation

$$0 = M(s) - s \tag{4}$$

We represent each of the above four pieces of information by a probability density function (PDF), with respective means b (for backscatter), o (for optical), p (prior), and 0 (for the devation of $M(s)$ from s) and respective covariance matrices $C(b)$, $C(o)$, $C(p)$, and $C(m)$ which quantify the respective uncertainties. We note that C_b and C_o include the uncertainty that arises from errors in the respective observation operators that cannot be corrected for by perfect state and parameter values.

For a compact notation we assemble all unknown quantities, i.e. the trajectory s and the parameters in the observation operators x_b and x_o into one long vector $\tilde{x}$ that we call the control vector. The retrieval is then achieved by find $\tilde{x}$ that minimises the cost function

$$J(\tilde{x}) = J_b(\tilde{x}) + J_o(\tilde{x}) + J_p(\tilde{x}) + J_m(\tilde{x}), \tag{5}$$

which is the sum of four contributions, one dedicated to each piece of information:

$$J_b(\tilde{x}) = \frac{1}{2} \sum_{i=1,n_b} (H_b(\tilde{s}_i, \tilde{x}_b, g_b) - b_i)^T C(b)^{-1} (H_b(\tilde{s}_i, \tilde{x}_b, g_b) - b_i), \tag{6}$$

where n_b is the number of S1 acquisitions;

$$J_o(\tilde{x}) = \frac{1}{2} \sum_{i=1,n_o} (H_o(\tilde{s}_i, \tilde{x}_o, g_o) - o_i)^T C(o)^{-1} (H_o(\tilde{s}_i, \tilde{x}_o, g_o) - o_i), \tag{7}$$

where n_o is the number of S2 acquisitions;

$$J_p(\tilde{x}) = \frac{1}{2} (\tilde{x} - p)^T C(p)^{-1} (\tilde{x} - p); \tag{8}$$

$$J_m(\tilde{x}) = \frac{1}{2} (M(s) - s)^T C(m)^{-1} (M(s) - s). \tag{9}$$

In our implementation we keep the dynamical model both simple and generic, and we deliberately allow the solution to infer a state vector that deviates from the model prediction. Such an approach is often called "weak-constraint variational" (*Zupanski*, 1997) in contrast to variational approaches that exclude deviations from the model trajectory, i.e where the model equations act as a strong constraint on the minimisation problem. The advantage of the weak-constraint approach (in particular with high uncertainty $C(m)$) is that it leaves high flexibility to fit the sentinel observations. In other words, our trajectory will be primarily determined by sentinel observations rather than by the dynamical model, i.e our output will be primarily an EO product rather than a model output constrained by observations.

The form of the model used here follows that of *Lewis et al.* (2012), who use a simple linear (more precisely a simple *affine*) model:

$$M(s) = As + b \ , \tag{10}$$

where the model parameters (i.e. the matrix A and the vector b) can be specified to suit a particular problem. In the following retrievals we set $A = I$ and $b = 0$ which equates to a simple zero-order model ("today is like tomorrow"). The consequence of using a model formulation like this is that it imposes a degree of temporal smoothness on the results, but also allows the information from each observation to influence the retrievals at other time steps. This is analogous to the temporal constraints on linear BRDF inversion described by Quaife and Lewis (2010).

3 Results and discussion

3.1 Retrievals

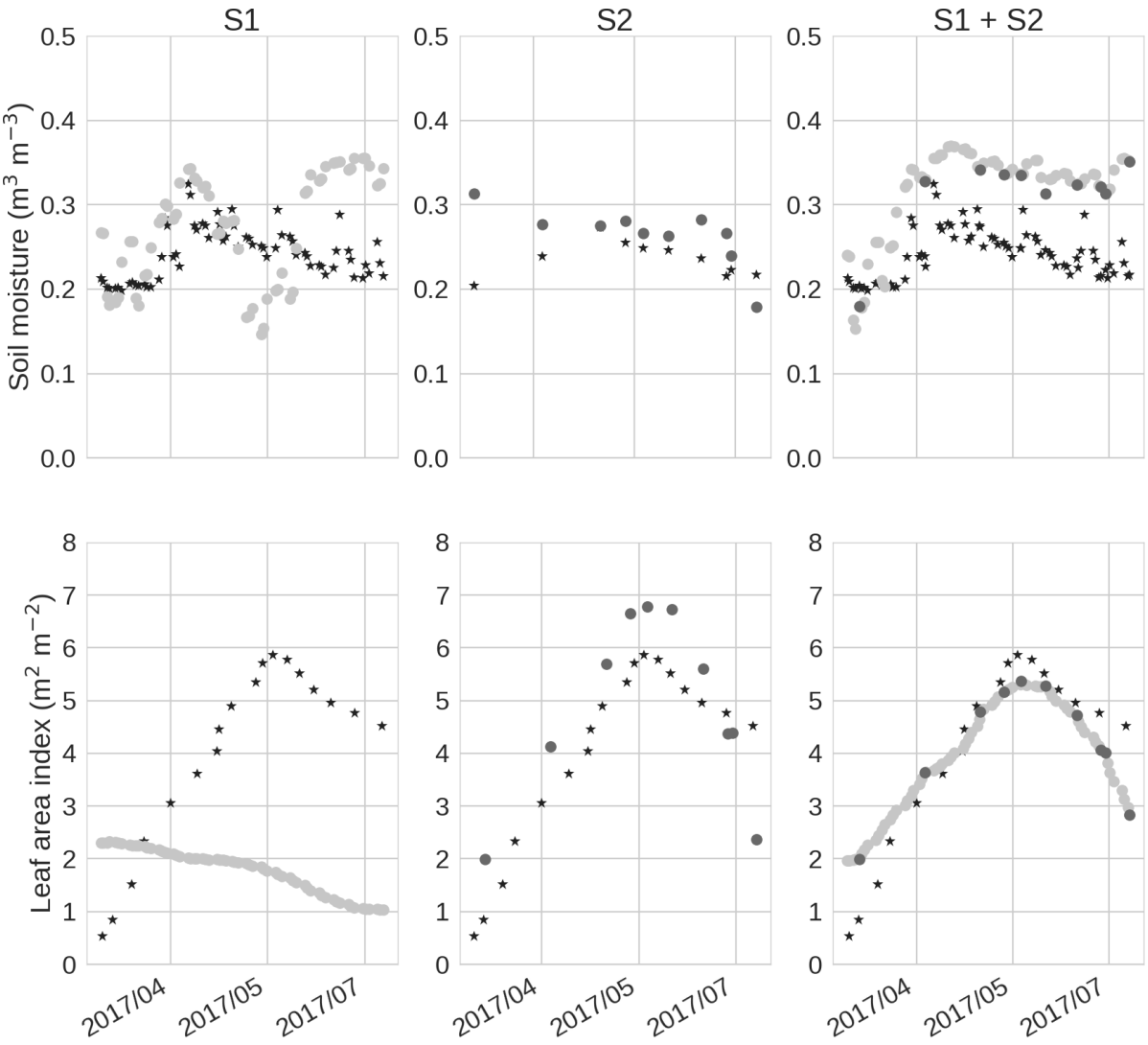

Figure 2: Comparisons of the retrievals for Sentinel–1 (left hand column) and Sentinel–2 (middle column) individually and jointly (right habd column). Field 508, "mid" sampling point. Stars indicate field observations. Dark points retrievals at Sentinel–2 acquisition times and light grey points retrievals at Sentinel–1 acquisition times.

For each of the evaluation points in described in 2.2 we compare retrievals of leaf area index and soil moisture for Sentinel–1 and Sentinel–2 separately and combined. Figure 2 shows the results for each of these combinations for the mid point of field 508. The general pattern here is indicative of the results for each of the evaluation locations and the full results are summarised using Taylor diagrams in Figure 5 and 6

and described later in this section. Sentinel–1 only retrievals tend to capture the mean soil moisture reasonably well but the variability, especially later in the growing season, is not well correlated with the field observations. We hypothesise that this is due to the poor representation of LAI in the in the retrieval, which is very poorly correlated with the field observations and is biased low for most of the growing season. The retrieval algorithm is adjusting the soil moisture to be too high to compensate for the low LAI. This is perhaps unsurprising and suggests a level of equifinality between the two variables in the SAR signal. The Sentinel–2 only retrievals show a much stronger correlation with LAI, representing the phenology of the crops well, with a small bias in the order of 1.0 LAI units. The soil moisture appears to represent the mean well but this is not borne out across all of the data points (see Figure 5) where in general the RMSE and correlation of the Sentinel–2 only soil moisture results is poor. For the joint retrieval the LAI matches very well. The influence of Sentinel-2 on the on the retrievals pulls the Sentinel–1 results into line via the dynamic model that is implemented in the retrieval algorithm. In turn this allows the soil moisture to take on a more realistic temporal evolution, albeit somewhat biased high and not exhibiting sufficient variability in this example.

Figures 3 and 4 show the joint retrieval results for each of the evaluation points for leaf area index and soil moisture respectively. For LAI the results are consistently good, in particular for fields 508 and 542. The phenological profile is well captured despite the fact that this is somewhat different between the fields. Field 542, for example, which is growing triticale starts its green up weeks later than the wheat growing in field 508 and this is well captured by the satellite data. Field 515 shows a positive bias in the retrieval results, which then appears to become unbiased toward the end of the season. The same is observed in the "mid" point of field 542. A consistent pattern observed for the wheat field is that the ground observed LAI appears to slow its decline toward the end of the season, whereas the retrieved LAI continues to reduce. This could be due to the effective LAI of the retrieval being reduced to compensate for a yellowing of the wheat foliage as the plant becomes senescent, where as the optical measurement technique used to estimate the LAI relies only on the amount of light intercepted and is hence to sensitive to changes in the leaf colour. However this pattern is not observed in the maize or triticale measurements and both of these species yellow as they pass maturity in much the same way as wheat.

Statistical summaries of the results for all nine points and the three possible combinations of sensors entering the retrievals are shown in Figure 5 for LAI and Figure 6 for soil moisture using Taylor diagrams (Taylor, 2001). The Taylor diagram allows for easy comparison of multiple experiments. The relative standard deviation of the retrievals to the ground observations is on both the x–axis and y–axis and increases radially from the origin. Correlation is shown on the polar axis such that the smaller the angle between a point and the horizontal axis the more correlated it is with the observations. Because there is an algebraic relationship between the relative standard deviation, correlation and RMSE it is also possible to plots the RMSE on the Taylor diagram; these are the radial contours the emerge from the 1.0 point of the x–axis. For LAI the Taylor diagram shows a clear picture. The Sentinel–1 only retrievals have very poor reproduction of

the variability in the ground–truth data and the RMSE is > 0.75 for all experiments. The Sentinel–2 only retrievals over–estimate the variability in the observations, but tend to have a correlation better the 0.8 and an RMSE > 0.5. For the joint retrievals the results are better than the individual cases for all points with RSME always less than < 0.5 and a correlation of better than 0.95. The Taylor diagram for the soil moisture is less clear. The join retrievals tend to have a a lower RMSE and higher correlation than the retrievals from either Sentinel on its own but this is not always the case. The joint retrievals also appear to suppress the variability quite significantly in most cases, where is the individual retrievals tend to contain too much variability.

3.2 Future work

One aspect of the current study that can clearly be improved upon is the inclusion of other variables from the respective radiative transfer models to be included in the retrieval. This was not attempted during this study as the complexity of the overall system was already high and our objective was to gain confidence in the LAI and soil moisture retrievals. Arguably the next most important variable to consider would be leaf water content as this has an impact on both the microwave signal and the short–wave infra red channels of Sentinel–2. We suggest that this should be the next step forward in similar studies looking to exploit synergies between these two Sentinel missions. Including leaf pigments such as chlorophyll should also be a priority and may help to improve retrievals as plants become senescent.

Prior probabilities required as inputs to the retrieval algorithm described in Section 2.4 in this study were assigned on the basis of expert elicitation, which is common practice in Bayesian inference, but more analytical methods could be employed for this purpose. Specifically understanding the errors in the Sentinel–2 level 2a surface reflectance and the microwave and optical radiative transfer models used as observation operators here have the potential to improve the retrievals. In addition being able to objectively specify the off–diagonal elements in the covariance matrices is well know to improve the results of such algorithms (Pinnington et al. 2016).

The particular choice of Sentinel–1 polarization and Sentinel–2 band combination employed was based on preliminary experiments that suggested these worked well with our choice of radiative transfer models. We do not intend to suggest that the combination used here will be the best in every situation or even optimal for this particular experiment. For Sentinel–2 for example, including all bands may lead to over confidence in the results and biasing the retrievals toward the optical data unless errors are correctly specified in the matrix $C(o)$. It is likely that this will need to include off–diagonal elements as well to represent correlated uncertainties in bands that are close to each other spectrally. In the examples in this paper $C(o)$ was set as a diagonal matrix.

The software used for the retrievals in this study was designed to allow flexibility but not computational efficiency. Ultimately the time series retrieval is likely too slow to be used across entire images. Consequently some further work is required to make this tool more efficient. Analysis of the computational performance of the retrievals (not shown here) revealed a large amount of time being used in the optical radiative transfer model,

despite the fact that there are relatively far fewer data points collected by Sentinel–2. The bulk of this is being used to perform multiple scattering calculations (ρ^M in Equation 1). A future evolution of the system we have presented should probably include a modified version of the Semi–Discrete model with a modified multiple scattering term.

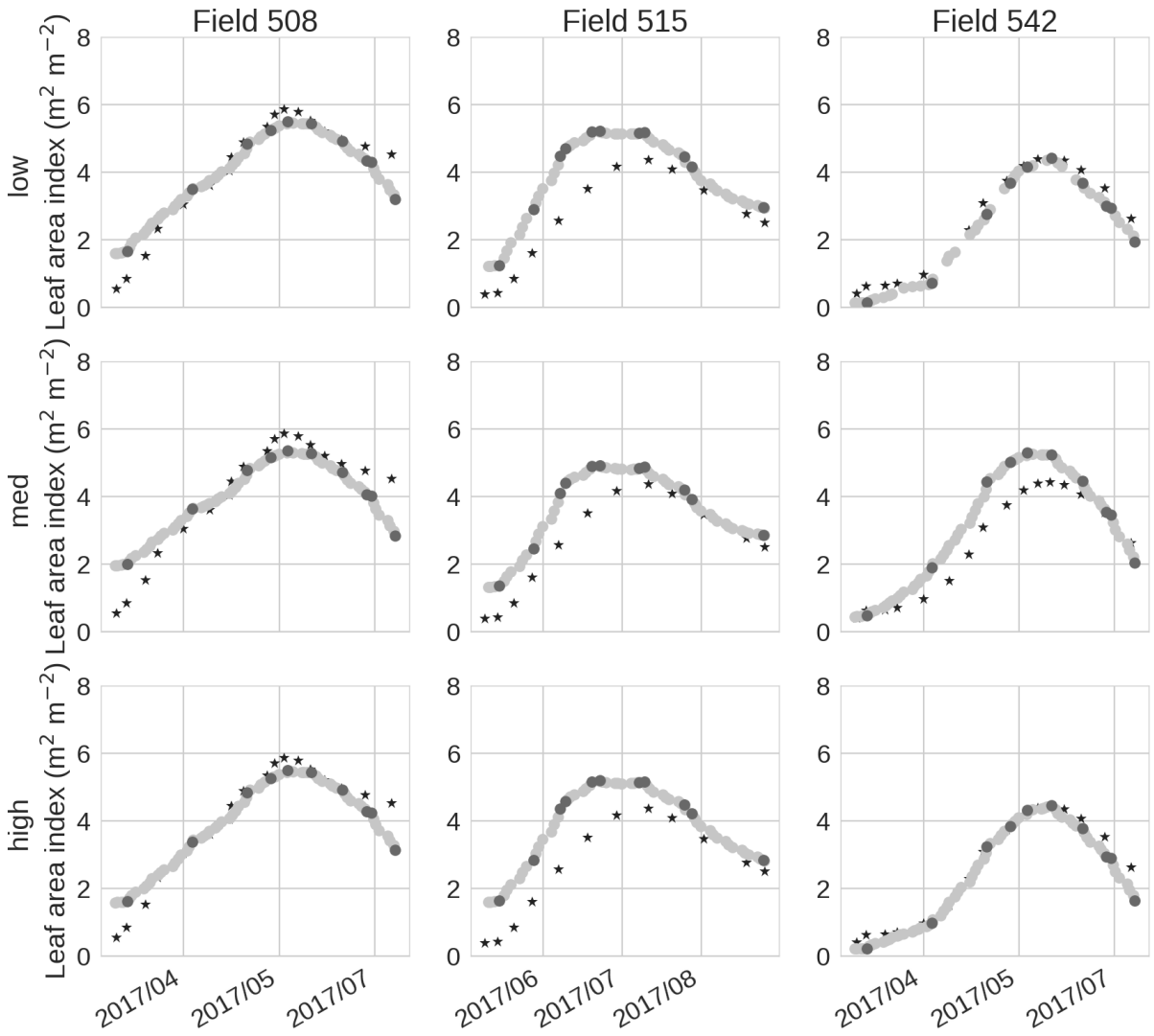

Figure 3: LAI retrievals using all Sentinel–1 and Sentinel–2 data from the 2017 growing season for each field (columns) and each sampling point (rows). Stars indicate field observations. Dark points retrievals at Sentinel–2 acquisition times and light grey points retrievals at Sentinel–1 acquisition times.

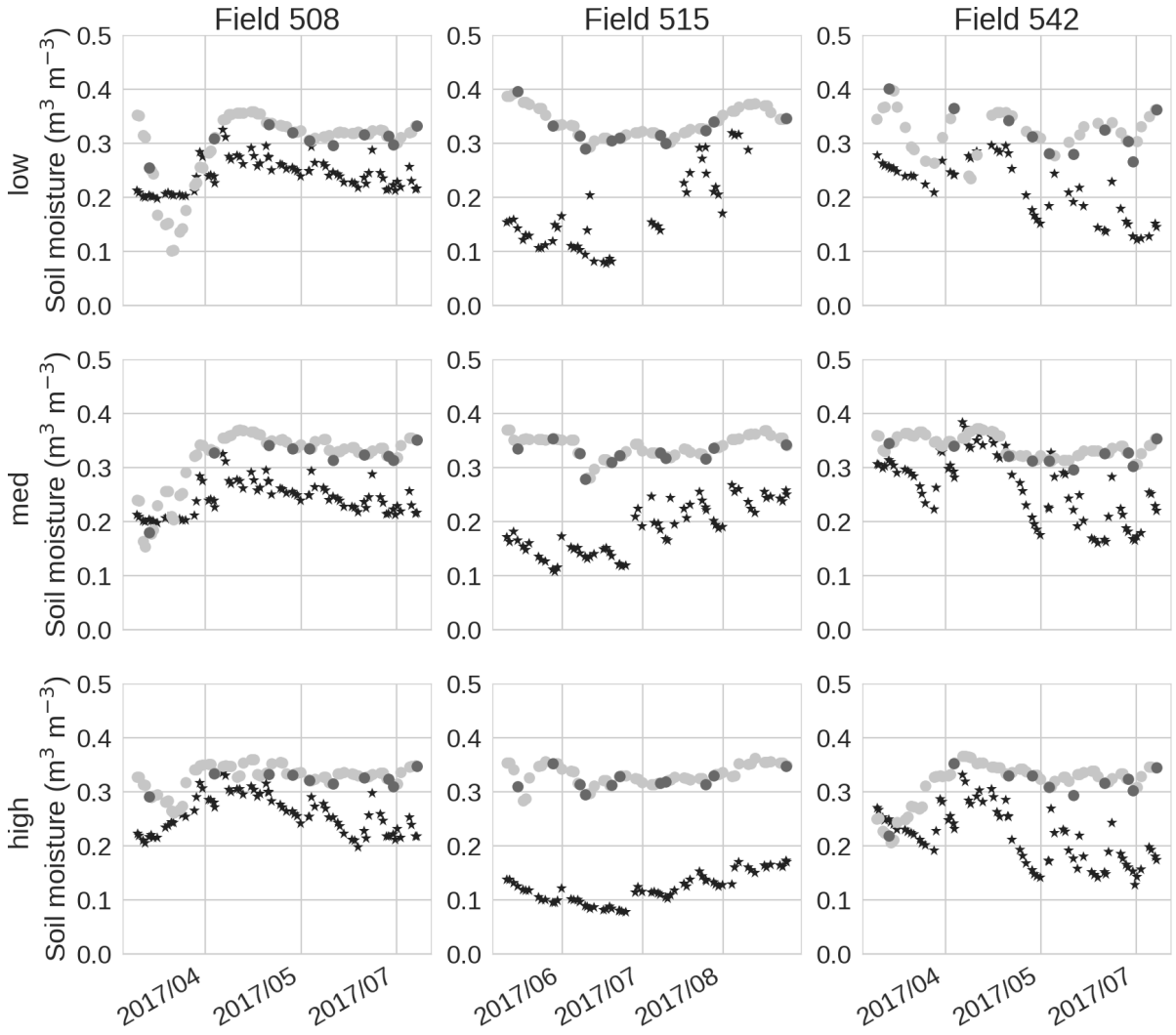

Figure 4: Soil moisture retrievals using all Sentinel–1 and Sentinel–2 data from the 2017 growing season for each field (columns) and each sampling point (rows). Stars indicate field observations. Dark points retrievals at Sentinel–2 acquisition times and light grey points retrievals at Sentinel–1 acquisition times.

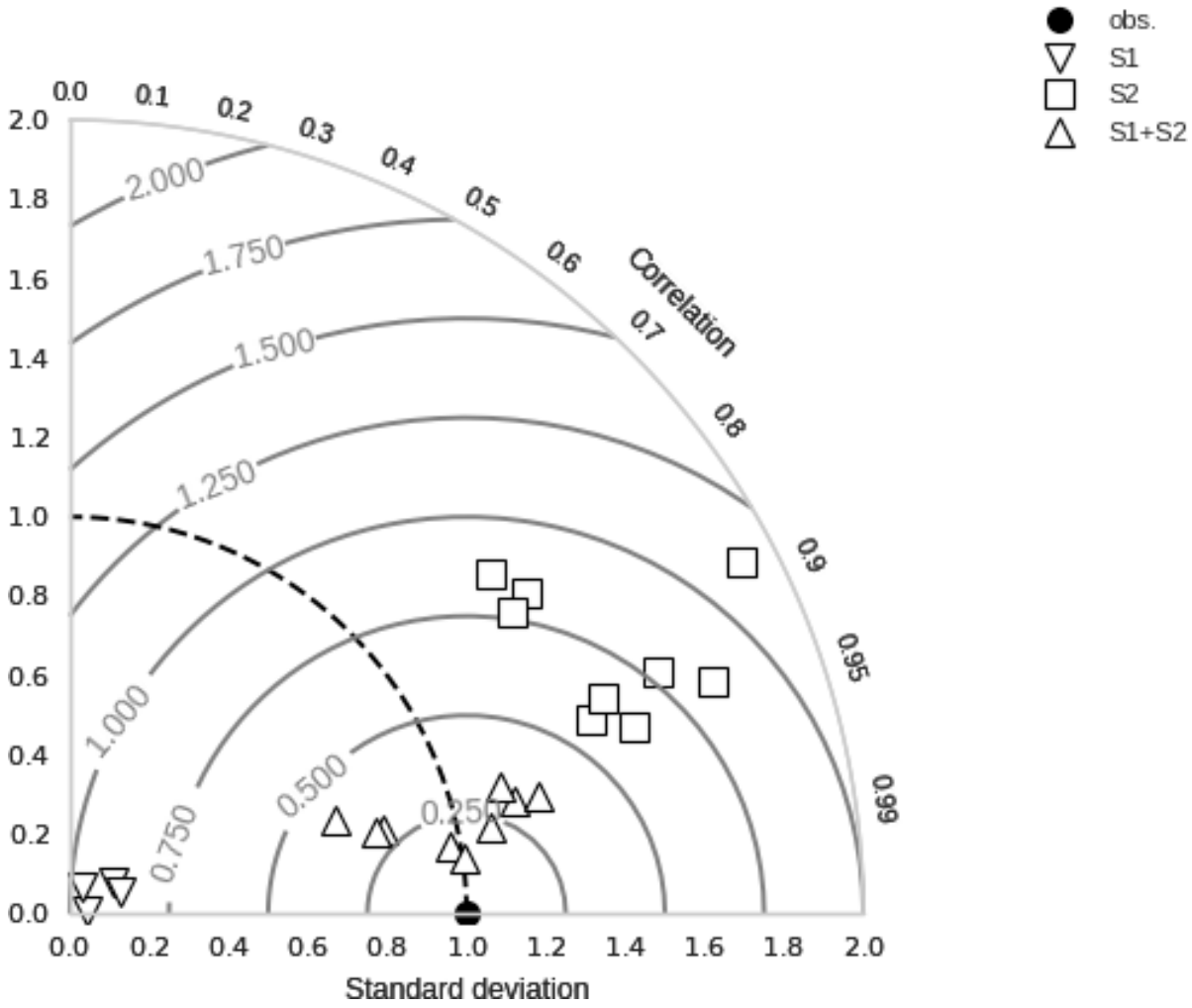

Figure 5: Taylor diagram showing summary results for LAI for each experiment. Distance from the origin indicates the level of variability compared to observations, with the dark dashed line representing the variability in the observations. The angle subtended with the horizontal axis represent correlation with the observations and the radial contours extending from the black dot represent relative RMSE. The closer a point to the black dot (which represent the observations) the better the retrieval has performed.

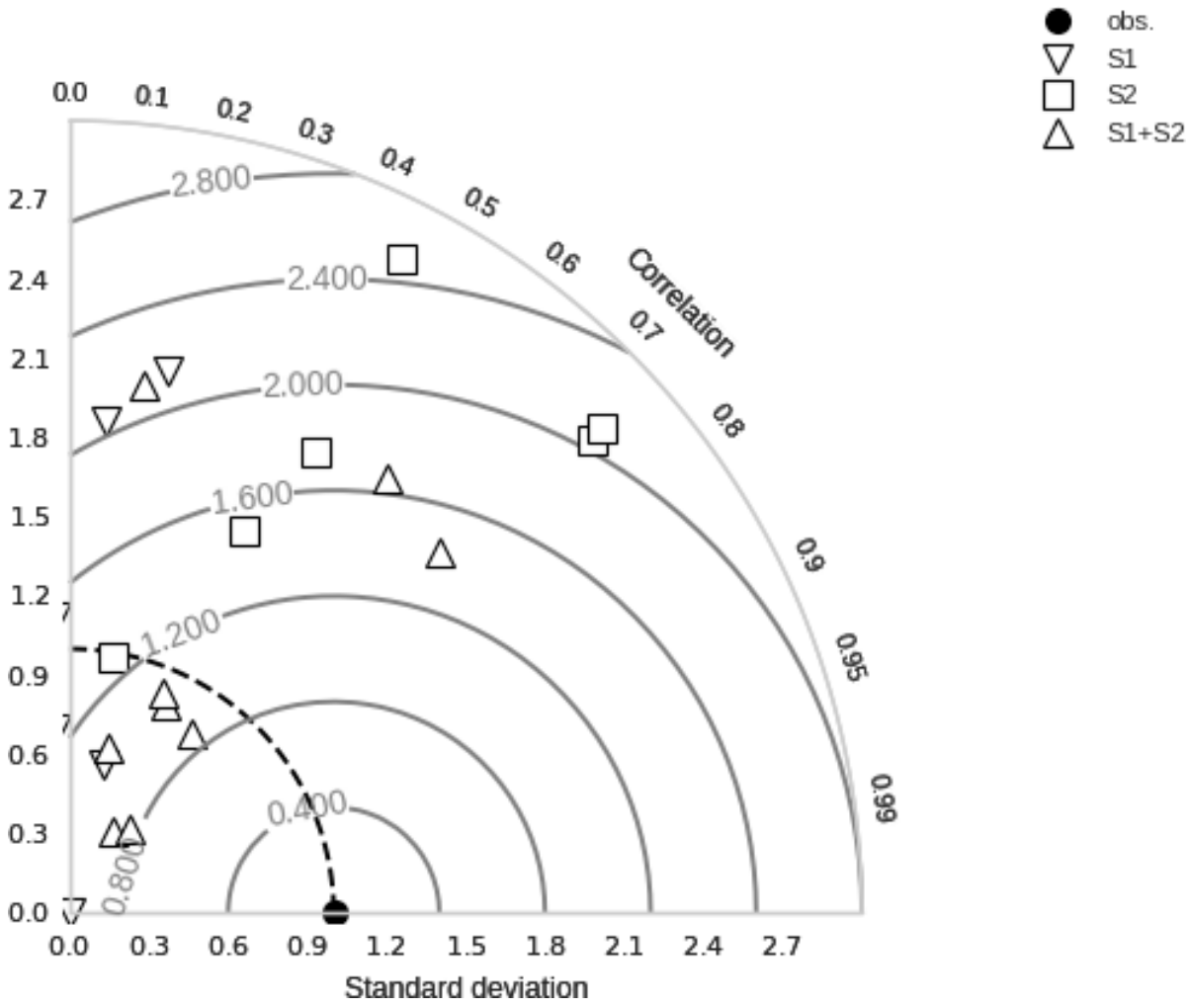

Figure 6: As Fig. 5 but for soil moisture.

4 Conclusions

We have demonstrated a joint retrieval algorithm for LAI and soil moisture from Sentinel–1 and Sentinel–2 data using physically based radiative transfer models. The inversion scheme uses adjoint versions of the computer code of these models to perform the cost–function minimisation and the values of the retrieved variables are constrained temporally using a dynamic model the prescribes the degree of smoothness in their evolution. By comparison against field observations from agricultural sites in Germany we showed that the joint retrieval improves estimates of leaf area index in every case compared to individual retrivals, and soil moisture in the majority of cases. There are very few examples of joint retrievals using physically based radiative transfer in the optical and SAR domains and none, to our knowledge, using Sentinel–1 and Sentinel–2. Our results show promise for future developments in this field

Acknowledgements

This project was funded by European Space Agency Contract 4000119682. Quaife and Pinnington were partly funded under by the UK NERC National Center for Earth Observation under NE/R016518/1. The initial concept for this work was created by our friend and colleague Alexander Loew who died shortly after the project started and to whom this manuscript is dedicated.

Bibliography

Attema, E., and F. Ulaby (1978), Vegetation modeled as a water cloud, *Radio Science*, *13*, 357–364 PP.

Bracaglia, M. (1995), A fully polarimetric multiple scattering model for crops, *Remote Sensing of Environment*, *54*(3), 170–179.

De Roo, R. D., Y. Du, F. T. Ulaby, and C. Dobson (2001), A semi-empirical backscattering model at l-band and c-band for a soybean canopy with soil moisture inversion, *IEEE Transactions on Geoscience and Remote Sensing*, *39*, 864–872 PP.

Disney, S. P., M.I., and P. Lewis (2003), Modelling the radiometric response of a dynamic, 3d structural model of scots pine in the optical and microwave domains, in *Proc. IEEE Int. Geos. RS Symposium*, vol. 6, pp. 3537– 3539.

Ferrazzoli, P., and L. Guerriero (1996), Passive microwave remote sensing of forests: A model investigation, *IEEE Transactions on Geoscience and Remote Sensing*, *34*(2), 433–443.

Jacquemoud, S., and F. Baret (1990), Prospect: A model of leaf optical properties spectra, *Remote sensing of environment*, *34*(2), 75–91.

Kaminski, T., B. Pinty, M. Voßbeck, M. Lopatka, N. Gobron, and M. Robustelli (2017), Consistent retrieval of land surface radiation products from eo, including traceable uncertainty estimates, *Biogeosciences*, *14*(9), 2527–2541, doi:10.5194/bg-14-2527-2017.

Karam, M. A., A. K. Fung, R. H. Lang, and N. S. Chauhan (1992), A microwave scattering model for layered vegetation, *IEEE Trans. Geosci. Remote Sensing*, *30*(4), 767–784.

Kim, S.-W., and J.-S. Won (2003), Measurements of soil compaction rate by using jers-1 sar and a prediction model, *Geoscience and Remote Sensing, IEEE Transactions on*, *41*(11), 2683–2686.

Kim, Y., and J. van Zyl (2001), Comparison of forest parameter estimation techniques using sar data, in *Proc. IEEE 2001 International Geoscience and Remote Sensing Symposium IGARSS '01*, vol. 3, pp. 1395–1397, doi:10.1109/IGARSS.2001.976856.

Lewis, P., P. Saich, M. Disney, B. Andrieu, C. Fournier, and S. Ljutovac (2003), Modelling the radiometric response of a dynamic, 3d model of wheat in the optical and microwave domains, in *Proc. IEEE Int. Geos. RS Symposium, 21-25 July 2003.*

Lewis, P., J. Gómez-Dans, T. Kaminski, J. Settle, T. Quaife, N. Gobron, J. Styles, and M. Berger (2012), An earth observation land data assimilation system (eo-ldas), *Remote Sensing of Environment*, *120*, 219 – 235, doi: http://dx.doi.org/10.1016/j.rse.2011.12.027, the Sentinel Missions - New Opportunities for Science.

Martinez, J. M., N. Floury, T. LeToan, A. Beaudoin, M. Hallikainen, and M. Maknen (2000), Measurements and modelling of vertical backscatter distribution in forest canopy, *IEEE Trans. Geosci. Remote Sensing*, *38*(2), 710–719.

Mattia, F., M. W. J. Davidson, T. Le Toan, C. M. F. D'Haese, N. E. C. Verhoest, A. M. Gatti, and M. Borgeaud (2003), A comparison between soil roughness statistics used in surface scattering models derived from mechanical and laser profilers, *Geoscience and Remote Sensing, IEEE Transactions on*, *41*(7), 1659–1671.

McNairn, H., J. Shang, X. Jiao, and B. Deschamps (2012), Establishing crop productivity using radarsat-2, *ISPRS - International Archives of the Photogrammetry, Remote Sensing and Spatial Information Sciences*, *XXXIX-B8*, 283–287, doi: 10.5194/isprsarchives-XXXIX-B8-283-2012.

N., G., P. B., V. MM., and G. Y. (1997), A semidiscrete model for the scattering of light by vegetation, *Journal of Geophysical Research: Atmospheres*, *102*, 9431–9446 PP.

Oh, Y., K. Sarabandi, and F. T. Ulaby (1992), An empirical model and an inversion technique for radar scattering from bare soil surfaces, *Geoscience and Remote Sensing, IEEE Transactions on*, *30*(2), 370–381.

Price, J. (1990), Using spatial context in satellite data to infer regional scale evapotranspiration., *IEEE Transactions on Geoscience and Remote Sensing.*, *28*(5), 940–948.

Prévot, L., H. Chauki, D. Troufleau, M. Weiss, F. Baret, and N. Brisson (2003), Assimilating optical and radar data into the stics crop model for wheat, *Agronomie*, *23*(4), 297–303.

Satalino, G., L. Dente, and F. Mattia (2006), Integration of meris and asar data for lai estimation of wheat fields, in *Proc. IEEE International Conference on Geoscience and Remote Sensing Symposium IGARSS 2006*, pp. 2255–2258, doi: 10.1109/IGARSS.2006.583.

Ulaby, T., F., and C. Elachi (1990), *Radar Polarimetry for Geoscience Appications*, Artech House, Inc.

Zupanski, D. (1997), A general weak constraint applicable to operational 4DVAR data assimilation systems, *Mon. Weather Rev.*, *125*(9), 2274–2292.